Exciton energies in shallow quantum wells and spin superlattices

J. Warnock
IBM Research Division, Thomas J. Watson Research Center, P.O. Box 218, Yorktown Heights, New York 10598

B. T. Jonker
Naval Research Laboratory, Washington, D.C. 20375-5000

A. Petrou, W. C. Chou,* and X. Liu†
Department of Physics and Astronomy, State University of New York, Amherst, New York 14260
(Received 19 April 1993)

We describe a general method of calculating exciton energies in shallow quantum wells. This technique is applicable to both single- and multiple-quantum-well systems, and is valid for both type-I and type-II systems, even under circumstances where the valence- and/or conduction-band offsets may be small compared to the exciton binding energy. Quantitative predictions of excitonic energies and relative intensities are made and compared with experimental data on a number of different shallow-well diluted magnetic semiconductor quantum well and superlattice systems. Based on these comparisons, it is shown that the model indeed provides a detailed description and analysis of the type-I–type-II transition and the behavior of excitons in a spin superlattice. In addition, the model also predicts and describes certain additional phenomena, such as metastable "above-gap" excitons which should exist in certain type-II systems. Also, reentrant type-I–type-II–type-I transitions are predicted under some circumstances.

INTRODUCTION

The atomic precision offered by advanced epitaxial techniques has produced new classes of tailored microstructures, where magnetic properties and band structure can be adjusted at will in order to highlight or elucidate the physical phenomena under study. This ability has allowed the fabrication of various dilute magnetic semiconductor (DMS) quantum-well and superlattice structures designed to probe different physical aspects of quantum confinement, reduced dimensionality of magnetic structures, and exciton or magnetic spin dynamics in two-dimensional (2D) systems. Studies of the type-I–type-II transition in quantum-well systems,[1,2] spin superlattices,[3–5] coupled quantum wells with tunable separating barriers,[6,7] the effect of dimensionality on magnetic behavior,[8] and the effects of confinement on carrier spin dynamics,[9–11] magnetic polaron formation,[12] and optically induced magnetization,[13] have all relied on the unique features of DMS-based microstructures. In particular, DMS heterostructures with very small "built-in" zero-field conduction- and/or valence-band offsets have emerged as a particularly interesting and important type of DMS microstructure, and these systems have received considerable attention in recent years. Not only has it been possible to build and study spin superlattices, but in principle it is possible to use these structures to accurately determine conduction- and valence-band offsets,[1,14] a topic which has seen considerable debate for many years. However, in order to accurately determine band offsets, the behavior of the exciton in a shallow confining potential must be accurately modeled. Approaches originally developed for deep quantum-well systems[15,16] will no longer work when the confining wells are small compared to the exciton binding energy. Variational approaches which use unaltered single-particle wave functions[17] are in general unsuited for use in shallow quantum wells where the Coulomb interaction plays a major role. Approaches which attempt to treat the electron-hole Coulomb interaction in an approximate fashion[14,18,19] are useful for relatively narrow quantum wells, as long as the conduction-band confining potential is large, but will not work in more general situations, nor will they allow accurate modeling of the excitonic wave functions in order to determine transition strengths. The approach can be improved somewhat by allowing a more general form for the hole wave function,[20] but still will be limited to situations where the wells are relatively narrow, with a large conduction-band offset (i.e., electrons tightly confined.)

In this work we describe the application of a hybrid variational approach to the modeling of excitons in shallow quantum-well systems. The technique overcomes the difficulties mentioned above, and allows calculations of excitonic energies with arbitrary valence and conduction-band potentials. The method is ideally suited for studying the magnetic field-induced type-I-type-II transition, and also applies to spin superlattice and spin quantum-well systems where both valence- and conduction-band offsets are generally small, and may be either positive or negative depending on the applied magnetic field and the spin of the electron or hole. In addition, the wave-function calculations are accurate enough to allow quantitative predictions to be made of relative transition strengths, a necessary feature for unambiguously determining conduction- and valence-band offsets simultaneously. The model also predicts and describes

the existence of metastable above-gap excitonic states in type-II systems, which are formed as a result of the Coulomb interaction between the electron and the hole. After describing the calculations, the model is applied to several different types of shallow well systems. In general the model is seen to provide an accurate description of the phenomena observed, allowing valence- and conduction-band offsets to be extracted, and providing a detailed understanding of the experimental data.

MODEL DESCRIPTION

To calculate exciton binding and confinement energies in shallow DMS quantum wells, a formalism is needed which extrapolates correctly to the three-dimensional limit, since in some cases confinement effects may be small in both conduction and valence bands. The model must be appropriate for type-II systems, and also for situations where strong confinement effects are present, since the magnetic-field-induced band splittings can result in relatively large band offsets, even when zero-field confinement effects are small. The transition from bulk-like behavior to quantum confinement is thus a more difficult problem than looking at limiting behavior in various situations. Previous treatments reported for the limit of tight quantum confinement in the conduction band, with small and variable valence-band offset need to be extended and refined to deal with spin superlattice systems and the type-I to type-II transition.

We start our treatment following the path of previous approaches[15] in the effective-mass approximation with an excitonic Hamiltonian (excluding the translational motion in the plane of the layers) given by

$$\mathcal{H}=\frac{p_{ze}^2}{2m_e}+\frac{p_{zh}^2}{2m_h}+\frac{p_x^2+p_y^2}{2\mu}-\frac{e^2}{\epsilon r}+V_q(z_e,m_{je})+V_q(z_h,m_{jh})\ . \tag{1}$$

Here m_e, $\mathbf{r}_e$, and p_{ze} are, respectively, the electron effective mass, position, and momentum in the direction perpendicular to the layers, and similarly, m_h, $\mathbf{r}_h$, and p_{zh} are, respectively, the hole effective mass, position, and momentum in the direction perpendicular to the layers. The relative electron-hole displacement is $\mathbf{r}=\mathbf{r}_e-\mathbf{r}_h$, μ is the reduced mass in the plane of the layers, and ϵ the dielectric constant. For DMS structures, the quantum-well potentials, $V_q(z_e,m_{je})$ and $V_q(z_h,m_{jh})$ for electron and hole, respectively, depend on both the z coordinate and the z spin components, m_{je} and m_{jh} for electrons and holes. These potentials contain the effect of the applied magnetic field through the giant spin splitting induced in the DMS layers.[21] The spin splitting in the DMS layer produces a spin-dependent band offset from the nonmagnetic to the DMS layer, in addition to the built-in zero-field band offset. The above Hamiltonian does not necessarily assume isotropic effective masses; μ depends solely on the in-plane electron and hole masses, where m_e and m_h as defined above refer only to the transverse masses. In the illustrative examples considered below, the in-plane and transverse masses are set equal for simplicity. However, in the fits to the experimental data separate masses are used for in-plane and perpendicular motion. We also assume that heavy-hole and light-hole bands are split apart in energy, and limit the discussion here to the treatment of the heavy-hole excitons ($m_j=\pm\frac{3}{2}$).

We next choose a generalized variational wave function in order to estimate the exciton binding energy and the nature of the wave function in the shallow quantum well. The trial wave function is of the form

$$\psi(r_\perp,z_e,z_h)=\phi_e(z_e)\phi_h(z_h)\phi_{e\text{-}h}(z_e-z_h,r_\perp)\ . \tag{2}$$

In particular, we choose $\phi_{e\text{-}h}(z_e-z_h,r_\perp)\propto\exp(-r/\lambda a_0)$ where λ is a variational parameter, and a_0 is the bulk exciton radius. Although the calculation is much easier if $\phi_{e\text{-}h}(z_e-z_h,r_\perp)$ is chosen to depend only on $r_\perp$ (i.e., the radial part is then separable from the rest of the wave function), that trial wave function is not appropriate for the situation where the confining potential is shallow in both conduction and valence bands, or for situations, where the well width is significantly wider than a_0. The form chosen here for $\phi_{e\text{-}h}(z_e-z_h,r_\perp)$ ensures that the solution extrapolates correctly to the bulk limit.

Given the form of the radial wave function chosen, and a particular value of λ, it is possible to find by numerical means a self-consistent set of functions $\phi_e(z_e)$ and $\phi_h(z_h)$, for electron and hole, respectively, which minimize the energy, E. These functions describe only part of the overall behavior of the excitonic wave function in the z direction since $\phi_{e\text{-}h}(z_e-z_h,r_\perp)$ also depends on z_e and z_h. To find $\phi_e(z_e)$ and $\phi_h(z_h)$, the approach taken here is an iterative method. First, electron and hole single-particle wave functions and energies are calculated as a starting point, and to provide a basis from which to determine the excitonic binding energy. Then, for the iterative wave-function calculation, we start by choosing a trial electron (or hole) wave function, $\phi_{1e}(z_e)$ which can be chosen as the single-particle ground-state wave function for the potential in question. Given this trial electron wave function, the corresponding hole transverse wave function is found which minimizes the overall excitonic energy. The hole wave function is found as the numerical solution to the following equation:

$$\langle\phi_{1e}(z_e)\phi_{e\text{-}h}(z_e-z_h,r_\perp)|\mathcal{H}|\phi_{1e}(z_e)\phi_{e\text{-}h}(z_e-z_h,r_\perp)\rangle\phi_{1h}(z_h)=\langle\phi_{1e}(z_e)\phi_{e\text{-}h}(z_e-z_h,r_\perp)|E|\phi_{1e}(z_e)\phi_{e\text{-}h}(z_e-z_h,r_\perp)\rangle\phi_{1h}(z_h)\ , \tag{3}$$

subject to the appropriate boundary conditions. (Note that the integrations implied by the above equation are meant to be carried out only over the variables z_e and $r_\perp$, and not z_h.)

If $\phi_{e\text{-}h}(z_e-z_h,r_\perp)$ had been chosen to depend only on $\mathbf{r}_\perp$, the function $\phi_{1h}(z_h)$ would be the solution to the single-

particle valence-band part of the Hamiltonian with the addition of an effective Coulomb potential determined by $\phi_{1e}(z_e)$. With the nonvariable-separable solution, the concept is the same, except that there are many more terms in the effective "Hamiltonian" for $\phi_{1h}(z_h)$. For example, the element

$$\langle \phi_{1e}(z_e)\phi_{e\text{-}h}(z_e-z_h,r_\perp)|V_q(z_e,m_{je})|\phi_{1e}(z_e)\phi_{e\text{-}h}(z_e-z_h,r_\perp)\rangle$$

is a function of z_h due to the z_h dependence of $\phi_{e\text{-}h}(z_e-z_h,r_\perp)$. The functional form for each of these terms is calculated for the given electron function, $\phi_{1e}(z_e)$, and then the hole function, $\phi_{1h}(z_h)$ is calculated. The function, $\phi_{1h}(z_h)$ minimizes the overall exciton energy given the particular value of λ and the functional form assumed for $\phi_{1e}(z_e)$. Associated with this hole wave function is an excitonic energy E_1. To improve the estimate of the excitonic energy, an improved electron wave function should be calculated, $\phi_{2e}(z_e)$, which takes account of the Coulomb potential generated by the hole. This function can be calculated using exactly the same methods and routines described above for calculating the hole wave function, and yields an exciton energy E_1' [The integrations expressed by Eq. (3) are now over z_h and $r_\perp$, leaving z_e as the independent variable.] The energy E_1' calculated will be lower than E_1 since the electron wave function is calculated as the exact solution to the effective potential in question, and thus yields a lower energy than that obtained with the previous trial electron wave function. Recalculation of the hole wave function will in turn yield a lower energy, and the procedure can be repeated until a close enough convergence is obtained. In most situations it was found that 4–5 iterations were sufficient. Physically, the iteration process used is analogous to a step-by-step process of mutual adjustment, where first the hole minimizes its energy by adjusting to the presence of the electron, then the electron minimizes its energy by adjusting to the hole-induced potential, after which the hole readjusts itself, continuing on until a self-consistent energy minimum is obtained. In this way, the lowest-energy electron and hole wave functions are obtained for a given value of λ. The parameter λ is then varied to find the overall energy minimum.

This technique avoids extensive numerical calculations, but provides the most accurate evaluation of the exciton energy with the chosen form of radial wave function. This feature is especially important during the type-I to type-II transition, where the final wave functions obtained may differ substantially from the single-particle wave functions. In some cases, the structure may be type II, but the Coulomb interaction may be strong enough so that the exciton is effectively type I. Furthermore, with only one variational parameter (λ) it is easier to check to make sure that the solution found indeed represents an overall minimum, rather than a local energy minimum. This is important as will be seen later, since situations may arise with metastable states representing a local energy minimum with respect to the variational parameter.

MODEL RESULTS

We next use the formalism developed above to study two different types of DMS quantum-well systems with shallow band offsets. In the first type of system, the zero-field conduction-band offset is large compared to the field-induced spin splitting, whereas the zero-field valence-band offset is small. In this case the system goes from type I (spatially direct recombination) to type II (spatially indirect) as the field is applied.[1,22] (Similar effects have been observed in $CdTe/Cd_{1-x}Mn_xTe$ quantum wells.[2]) In the second type, both conduction- and valence-band offsets are small at zero field. In this system, the so-called "spin superlattice,"[3] transitions remain direct but the effect of the magnetic field is to create a spin-dependent confining potential which results in a spatial separation of the excitonic spin states.[4,5] In both systems strongly asymmetric spin splittings are observed as a result of the spatial separation of spin components in the valence band.

To illustrate the behavior observed in a DMS quantum-well or superlattice structure with small zero-field valence-band offset but large conduction-band offset, we consider the structure illustrated schematically in Fig. 1. The calculations are easily extended to superlattice and more complicated structures simply by changing the appropriate boundary conditions and confinement potentials where necessary. Thus the phenomena observed in this simple two-layer structure serve to illustrate the general behavior of this class of systems. The zero-field ground-state electron and hole probability distributions are also shown in Fig. 1. In this and following discus-

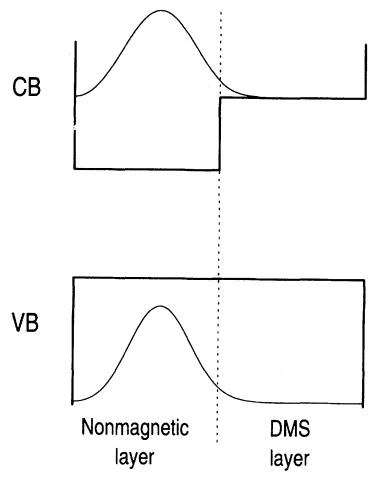

FIG. 1. Quantum-well potential used as an example for model calculations. Magnetic (barrier) and nonmagnetic (well) layer thicknesses are both equal to $3a_0$. CB well depth is twice the bulk exciton binding energy E_0, VB offset is zero at zero field. Electron and hole probabilities are shown as calculated by the model and discussed in the text.

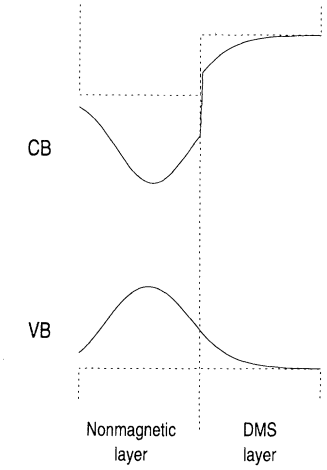

FIG. 2. Calculated CB and VB potentials at zero field including the effect of the Coulomb interaction. Dashed lines indicate the bare quantum-well potentials and the separation between layers. Solid lines show the effective potential seen by electron (CB) and hole (VB).

sions, the probabilities are illustrated by averaging over all variables except one specific z coordinate, and then plotting the resultant quantity as a function of that z coordinate. For example, to describe the probability of finding the electron at a given value of z_e, the function $|\tilde{\psi}(z_e)|^2$ is plotted by integrating over all hole z_h coordinates and relative radial coordinates, i.e.,

$$|\tilde{\psi}(z_e)|^2 \equiv |\phi_e(z_e)|^2 \int dz_h d^2 r_\perp |\phi_h(z_h)|^2 |\phi_{e-h}(z_e - z_h, r_\perp)|^2 . \tag{4}$$

The corresponding procedure is also followed for the hole probabilities. From Fig. 1 it is evident that the hole is confined by the Coulomb interaction even in the absence of a confining potential.[14,18] The Coulomb well seen by the hole (i.e., integrating over electronic and relative radial coordinates) shows (Fig. 2) how the electron confinement results in a corresponding hole confinement. The effective quantum-well potential seen by the electron is also distorted by the Coulomb attraction.

As the magnetic field is applied, the valence and conduction bands split as shown in Figs. 3 and 4. In the conduction band, the effect is minimal, due to the large zero-field band offset. However in the valence band, a negative band offset is induced for the lowest-energy spin state (i.e., the system becomes type II), while a positive confining potential appears for the other spin state (type I). (Similar effects will be observed for the light-hole spin states, which are separated from the heavy-hole states by the presence of uniaxial strain.) At low magnetic fields (where ΔE_h, the valence-band spin splitting is less than twice the exciton binding energy, E_b) the system remains effectively type I for both spin states, since the spin-dependent potential is not yet large enough to overwhelm the Coulomb interaction, which acts similarly to an additional confining potential. This situation is shown in Fig. 3.

As the field increases, the situation becomes more interesting. At a high enough magnetic field, the lowest-energy excitonic state $(m_{jh} = -3/2, m_{je} = -1/2)$ is literally pulled apart, as shown in Fig. 4. This spin state becomes genuinely type II while the other spin state $[(m_{jh} = +3/2, m_{je} = +1/2)]$ is type I with the holes tightly confined to the nonmagnetic layer. The binding energies of the two spin states are substantially different, changing as a function of magnetic field as shown in Fig. 5. The transition intensities or oscillator strengths also show different behavior, as illustrated in Fig. 6.

At very high fields, the conduction-band splitting may be large enough to cause a reentrant transition back to type-I behavior. Although this has yet to be observed experimentally, this type-I–type-II–type-I transition should be observable in material systems presently available provided the well widths and compositions are carefully chosen. In Fig. 5 a gradual increase in binding energy is seen $(-3/2, -1/2$ exciton state) at very large values of the spin splitting. This reflects the lowering of the conduction-band barrier, and the resulting increase in electron-hole wave-function overlap. The oscillator strengths also begin to increase in this region (Fig. 6). The onset of this transition will depend on the initial zero-field conduction-band offset, being shifted to higher fields with increasing zero-field offset. A clear signature of such a transition would be an intensity of the $(-3/2, -1/2)$ exciton component which falls rapidly at low fields, but recovers substantially at higher fields.

It is interesting to focus on the type-I to type-II transi-

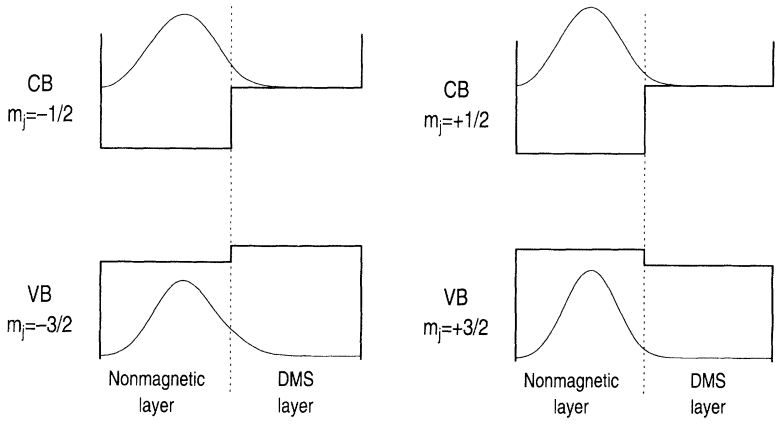

FIG. 3. DMS quantum wells in a weak magnetic field. VB offset is $\pm E_0/2$. Due to the large CB offset and the Coulomb interaction, both excitonic spin states are still type-I-like even though the quantum-well potential is type II.

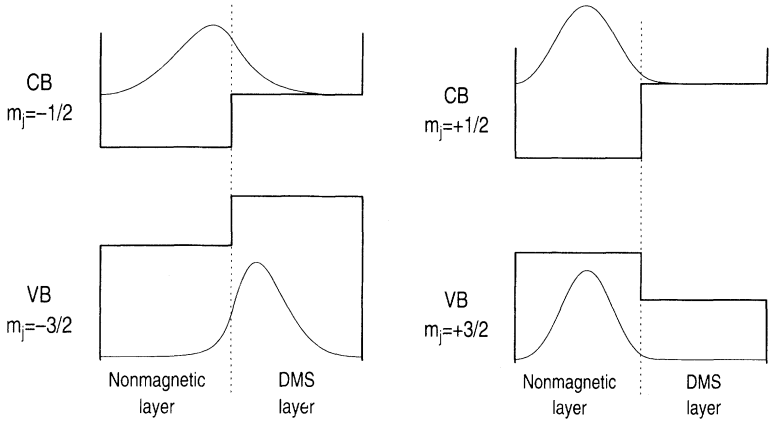

FIG. 4. Exciton in a DMS quantum well at high magnetic field. VB offset is $\pm 2E_0$. The lower-energy excitonic spin state is type II $(-3/2, -1/2)$, while the other state is type I $(+3/2, +1/2)$.

tion in the lower-energy spin state. In the transition there may occur a region of metastability, which can persist even to high fields depending on the details of the structure. This metastability is most likely to occur in systems with wide wells and strong conduction-band confinement. To look more closely at this transition region in such a structure, we calculate the exciton energy as a function of λ, the variational parameter which measures the correlation between the electron and hole wave functions. For the type-II structure in question, two minima are observed (Fig. 7), one near $\lambda=1$, and one broad minimum near $\lambda=4.0$. To see that this is not an artifact of the variational scheme used, the wave functions are determined at each of the two minima. The physical nature of the exciton wave function is found to be very different at each of these two regions. Near $\lambda=1$ the exciton is more bulklike, with both hole and electron wave functions confined to the nonmagnetic layer, similar to the zero-field situation. The Coulomb attraction from the electron provides a local potential well for the hole, which is thereby confined to the well layers in close proximity to the electron. For values of λ smaller than 1, this bulklike type-I excitonic wave function provides the lowest-energy solution. However, as λ is increased past 1, the energy increases rapidly, until a point is reached where it is energetically favorable for the hole to be confined to the barrier. The lowest-energy wave function for larger values of λ is that of a type-II exciton. The energies of both type-I and type-II excitons are shown in Fig. 7 as dotted lines, with the solid line indicating the overall lowest energy (type I or type II) as a function of λ. In the situation under consideration here, the type-II minimum is lower in energy than the type-I bulklike exciton energy. However, there is no easy relaxation path from the bulklike type-I excitonic state to the type-II indirect exciton state. The hole must tunnel through a Coulomb barrier. This barrier will exist as long as confinement effects are such that the electron wave function is concentrated at the center of the well, although the Coulomb potential will not be strong enough to keep the hole confined in thin well layers.

If both conduction- and valence-band offsets are small at zero field, then confinement potentials in both bands

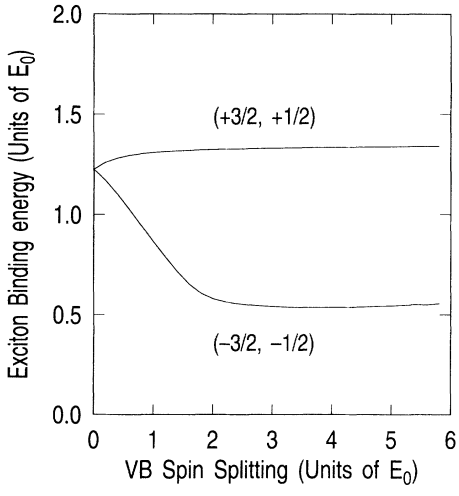

FIG. 5. Excitonic binding energies as a function of valence-band spin splitting. Even the type-II exciton has non-negligible binding energy due to the penetration of the wave functions into the layers and the correlation between electron and hole wave functions in the *xy* plane.

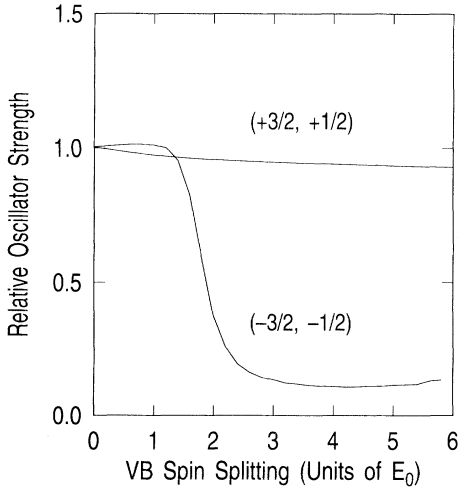

FIG. 6. Excitonic oscillator strength as a function of the valence-band spin splitting.

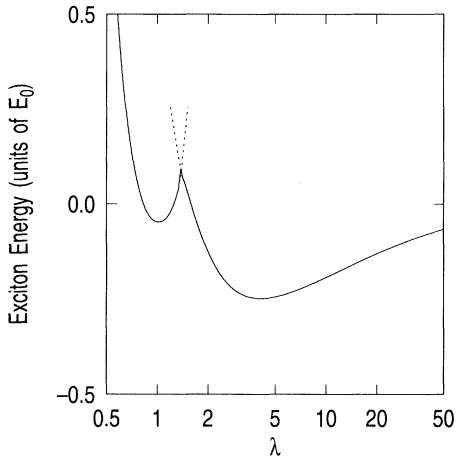

FIG. 7. Excitonic energy as a function of its radius in the plane of the layer (λa_0 is the effective exciton radius). Well width is $9a_0$, barrier is $3a_0$, VB offset is $-1.25E_0$. Note two minima; one corresponding to a type-I exciton in the nonmagnetic layer, and the other corresponding to a type-II exciton with the hole in the DMS layer.

are solely determined by the effect of the applied magnetic field. An extended structure of this type, consisting of alternating magnetic and nonmagnetic layers, forms the so-called "spin superlattice"[3] with a tunable minigap. In addition, the exciton wave functions are spatially separated according to their spin state, with one spin state confined primarily to the magnetic layer, and the other in the nonmagnetic layer. An example of this behavior is shown in Fig. 8, for a simple two-layer system (other systems such as superlattices can be treated by substituting the appropriate boundary conditions, and the phenomena observed are qualitatively similar). With no band offset at zero field and equal magnetic and nonmagnetic layer thicknesses, exciton binding energies, and transition strengths are the same for each spin state. However, small residual (i.e., zero field) band offsets or differing layer thicknesses would be expected to result in somewhat asymmetric behavior in most experiments.

EXPERIMENTAL RESULTS

A variety of quantum-well and superlattice systems were studied in order to explore experimentally the behavior discussed above. In general, the single quantum-well samples consisted of a nonmagnetic layer sandwiched between two magnetic layers, and the multiple quantum-well samples consisted of several periods of alternating magnetic and nonmagnetic layers. Most of the samples studied were Fe-based DMS structures,[23] although studies of Mn-based compounds were also carried out to ensure that the results were not somehow specific to the Fe-based microstructures. For the model calculations, the spin splitting in the magnetic layers was determined from magnetoreflectivity measurements on thick magnetic epilayers with magnetic ion concentrations equal to that in the DMS layers in the microstructures. A list of the samples used in this work as well as some of their parameters are given in Table I. Details on the growth of these structures and on the magnetoreflectivity setup used to study the excitons have been given elsewhere.[24] The first type to be discussed (samples 1, 2, and 3 in Table I) had relatively large conduction-band offsets at zero field, i.e., large compared to the conduction-band spin splittings observed at the highest attainable fields. On the other hand, zero-field valence-band offsets are small enough to be overcome by the field-dependent splitting, allowing the observation of the type-I–type-II transition.[1,22] The field-dependent exciton spin splittings are shown in Fig. 9. The asymmetric spin spitting is a result of the spin separation occurring in the valence band. The lowest-energy spin state $[(-3/2,-1/2)]$ becomes localized in the magnetic layer, and it shows the large field-dependent energy redshift typical of DMS materials. The other spin state $[(+3/2,+1/2)]$ is confined to the nonmagnetic layer and its energy shifts only slightly as a function of applied field.

The curves shown in Fig. 9 are calculated for all three samples assuming an infinite potential barrier at each of the sample boundaries. The bulk exciton binding energy E_0, in-plane and perpendicular effective masses are taken from the literature, with net valence- and conduction-band offsets treated as fitting parameters. The best fit was obtained with zero-field offsets of -12.5 and $+20$ meV

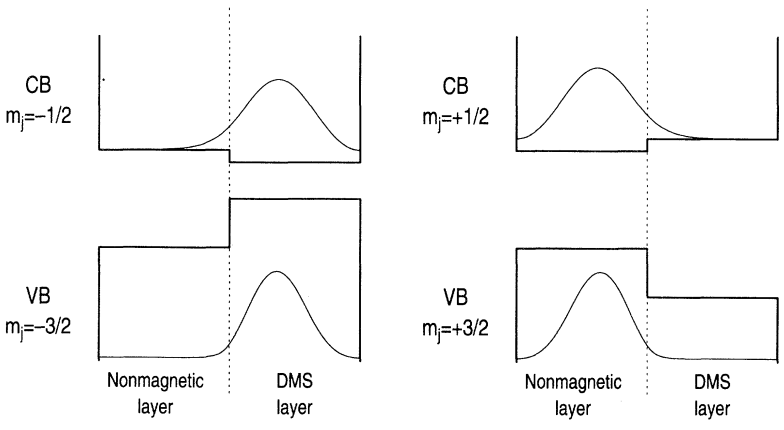

FIG. 8. Spin quantum well (no zero-field CB and VB offsets) at a finite field. The $(-3/2,-1/2)$ exciton is in the DMS layer, the $(+3/2,+1/2)$ exciton is in the nonmagnetic layer.

TABLE I. Sample parameters.

Sample number	Type	x	Layer thicknesses (Å)
1	$Zn_{1-x}Fe_xSe/ZnSe/Zn_{1-x}Fe_xSe$ quantum well	$x=10\%$	100/100/100
2	$Zn_{1-x}Fe_xSe/ZnSe/Zn_{1-x}Fe_xSe$ quantum well	$x=10\%$	100/150/100
3	$Zn_{1-x}Fe_xSe/ZnSe/Zn_{1-x}Fe_xSe$ quantum well	$x=10\%$	100/200/100
4	$Zn_{1-x}Mn_xSe/ZnSe/Zn_{1-x}Mn_xSe$ quantum well	$x=8.8\%$	348/116/116
5	$Zn_{1-x}Fe_xSe/ZnSe/Zn_{1-x}Fe_xSe$ quantum well	$x=1\%$	100/100/100
6	$Zn_{1-x}Fe_xSe/ZnSe/Zn_{1-x}Fe_xSe$ superlattice	$x=1\%$	(96/96/)×4

in the valence and conduction bands, respectively. This means that the structure is weakly type II at zero field, although the exciton binding energy is large enough so that both hole and electron wave functions are mainly in the nonmagnetic "well" layer, and the exciton is type I in character. It is interesting to note the significance of excitonic effects in this system; calculations which do not include the effect of the Coulomb interaction lead to a much smaller value of the valence-band offset.[4] The strain-induced energy shifts and band offsets can be calculated and subtracted from the band offsets determined above to yield the intrinsic or unstrained band offsets. However, uncertainties in the deformation potentials and the actual value of strain in the samples makes such calculations useful only for rough estimates. In this case it appears that the valence-band energy increases with increasing Fe concentration, as does the conduction-band energy. The net effect is an increase in the band gap, since the conduction-band energy increases more rapidly.

The intensity ratios of the two heavy-hole excitonic transitions for samples 1, 2, and 3 are shown in Fig. 10, along with the theoretical curves. The model correctly describes the trends observed in the data. In this situation the asymmetric intensity ratio is evidence that the lowest-energy excitonic state becomes type II upon application of the magnetic field. Without the intensity data, conduction-band and valence-band offsets are considerably more ambiguous, since to some extent the effect of changing the valence-band offset could be compensated for by changing the conduction-band offset in the opposite direction. However, it was found that the predicted intensity ratios were quite sensitive to the initial conduction-band offset, while being relatively insensitive to the initial valence-band offset. A few meV change in the conduction-band (CB) offset could result in a factor of 2 change in the intensity ratio for the sample with the narrowest nonmagnetic layer. This is because the intensity ratio reflects the overlap of the electron wave function into the magnetic layers, while the overlap of the lowest-energy spin hole wave function into the nonmagnetic layer is less important due to the higher effective mass of the hole, and the large spin-dependent valence-band (VB) offset. The predicted intensity ratios and/or extracted CB offsets are also sensitively dependent on the exact

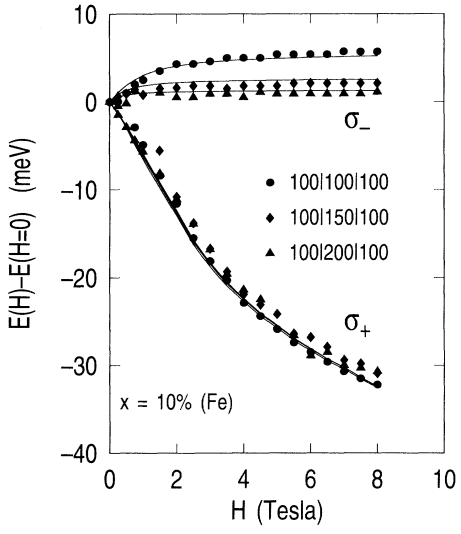

FIG. 9. Experimental data and model calculations for samples 1, 2, and 3, showing excitonic energy as a function of applied magnetic field. The set of numbers by the symbol keys refers to the $Zn_{1-x}Fe_xSe/ZnSe/Zn_{1-x}Fe_xSe$ layer thicknesses in the quantum-well structure.

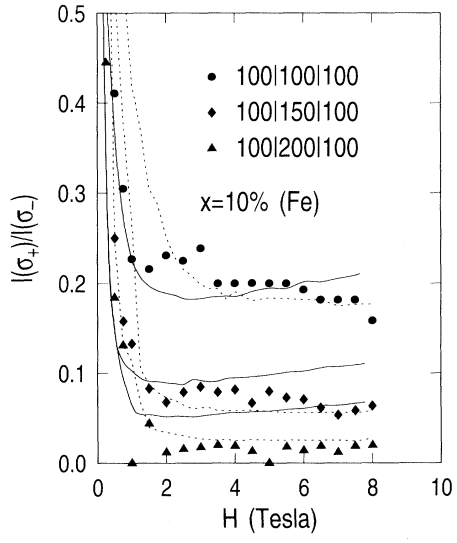

FIG. 10. Experimental and model calculations for samples 1, 2, and 3 showing intensity ratio vs magnetic field. Dashed lines indicate an alternate fit to the data, with well widths arbitrarily reduced by 25 Å in order to show the sensitivity of the fit to well width. The set of numbers by the symbol keys refers to the $Zn_{1-x}Fe_xSe/ZnSe/Zn_{1-x}Fe_xSe$ layer thicknesses in the quantum-well structure.

width of the nonmagnetic layer. Also shown in Fig. 10 (dashed lines) is an example of a fit to the data assuming slightly narrower wells (each well is assumed to be 25 Å less than its nominal value). In this case, valence-band and conduction-band offsets are readjusted to fit both the energy and intensity data, and offsets of −9 and 27 meV are obtained, respectively, for valence and conduction bands. The CB offset obtained is considerably larger than before, since with narrower wells the potential well must be made deeper to maintain the same barrier penetration of the electron wave function, and hence intensity ratio.

One other sample of this class was studied, but from another material system ($ZnSe/Zn_{1-x}Mn_xSe$, sample 4 in Table I). The initial band offsets are expected to be similar, but spin splittings are larger. These data are shown in Fig. 11, where the exciton energy for both spin states is plotted as a function of magnetic field. In this case offsets of −12 and 30 MeV, respectively, for valence and conduction bands were found to adequately describe the data. The similarity between this sample and the Fe-based materials described above is further evidence that the phenomena observed here are a general manifestation of the valence-band spin-state spatial separation which occurs in these systems, rather than a peculiarity of a given materials system.

A second group of samples studied consisted of quantum wells and superlattices where both VB and CB zero-field offsets were small. These samples are true "spin superlattices" (Ref. 4), or "spin quantum wells" where spin-dependent potentials play the dominant role in the confinement of both electrons and holes. At high enough magnetic fields, excitons are separated spatially according to spin state. The first sample of this type (sample 5) is a single quantum-well sample similar to sample 1, except with only 1% Fe in the barriers instead of 10% (well and barrier thicknesses were all 100 Å). The field-induced splitting is somewhat less (Fig. 12) due to the reduced Fe concentration, but it shows the same general features as observed for sample 1. However, the intensity ratio shows a much different behavior (Fig. 13), increasing slightly, then falling back to remain near 1. This behavior is consistent with much smaller zero-field valence- and conduction-band offsets and the fits shown in Figs. 12 and 13 were obtained with offsets of 0 and 5 meV, respectively, in valence and conduction bands. Again the model quantitatively describes the field-induced spin splitting while also describing the trends shown in the intensity data. In Fig. 13, the intensity ratio increases initially at low fields due to the finite CB offset which tends to keep the exciton localized in the nonmagnetic layer. The oscillator strength of the $(-3/2, -1/2)$ exciton initially increases as the small negative valence-band offset stretches the hole wave function which was initially localized by the Coulomb interaction. The extension of the hole wave function then more closely matches that of the electron, and the oscillator strength is increased. At high fields the higher experimentally observed intensity ratio would tend to imply a somewhat smaller CB offset than the 5 meV used in the fit. However, with a smaller CB offset, a worse fit is obtained to the energy data; the model would predict more excitonic spin splitting than is actually observed (the degree of spin splitting in the magnetic layers is taken from separate measurements on thick epilayers, and is not treated as a parameter in these fits).

Finally, a multiquantum well (MQW) sample was studied. To treat this case theoretically, the model can be altered to change the boundary conditions, or alternatively the model can be used in the same form treating several alternating layers instead of just two or three as required for the previous samples. For samples where the layer

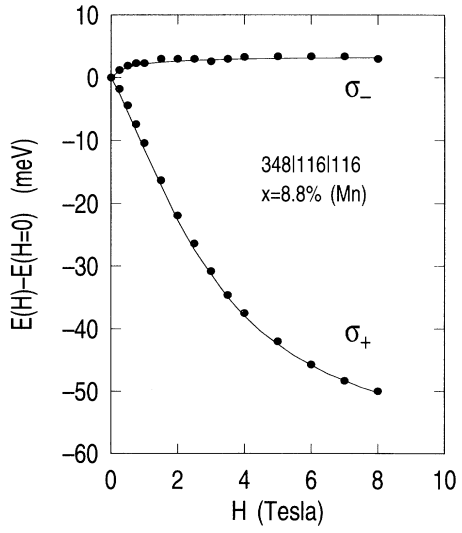

FIG. 11. Experimental and model calculations for sample 4, excitonic energy as a function of magnetic field. The set of numbers by the symbol keys refers to the $Zn_{1-x}Mn_xSe/ZnSe/Zn_{1-x}Mn_xSe$ layer thicknesses in the quantum-well structure.

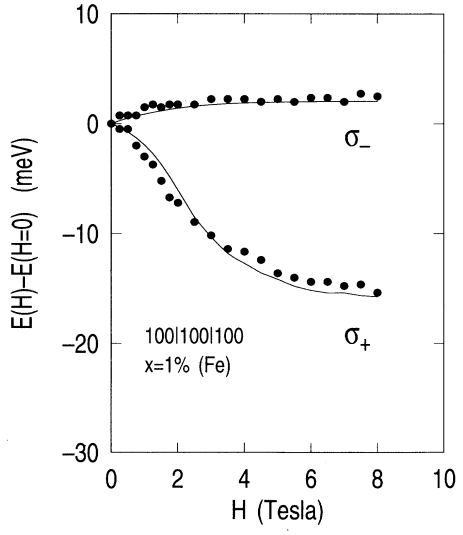

FIG. 12. Experimental and model calculations for sample 5, excitonic energy as a function of magnetic field. This sample is an example of a spin quantum well, with minimal zero-field conduction- and valence-band offsets. The set of numbers by the symbol keys refers to the $Zn_{1-x}Fe_xSe/ZnSe/Zn_{1-x}Fe_xSe$ layer thicknesses in the quantum-well structure.

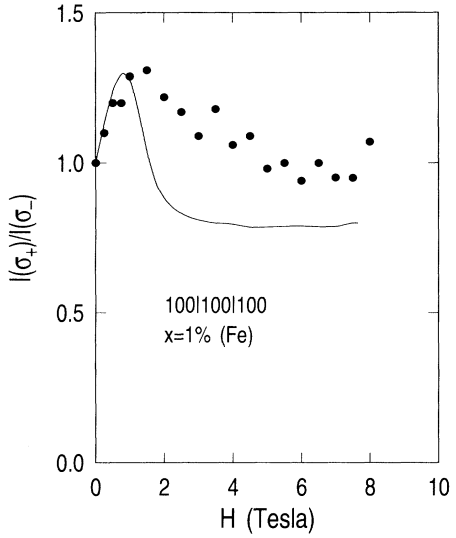

FIG. 13. Experimental and model intensity ratio calculations for spin quantum well sample 5. The set of numbers by the symbol keys refers to the $Zn_{1-x}Fe_xSe/ZnSe/Zn_{1-x}Fe_xSe$ layer thicknesses in the quantum-well structure.

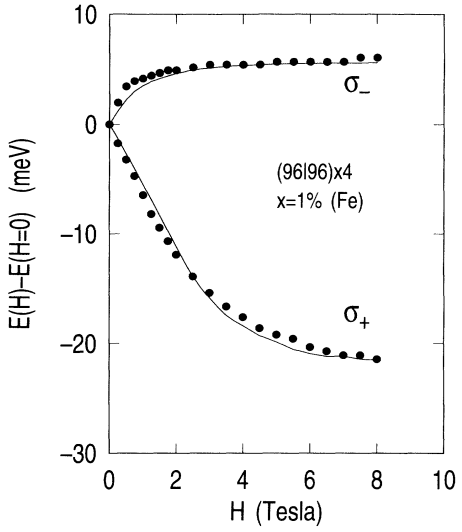

FIG. 14. Spin superlattice excitonic energy as a function of magnetic field. The set of numbers by the symbol keys refers to the $Zn_{1-x}Fe_xSe/ZnSe$ layer thicknesses in the superlattice structure.

thicknesses were comparable to or larger than the excitonic diameter, this method was found to be adequate, and only 2–3 periods were required to accurately predict the ground-state energy. The experimental results are shown along with the model results in Fig. 14 for sample 6. This is a 4-period MQW sample with 96-Å well and barrier layers, and $x=1\%$ (Fe) in the layers. Again, the model is able to describe the excitonic energy as a function of field. However, there are some discrepancies noted here between these results and the results obtained for the previous single quantum-well sample (sample 5). For the MQW sample, the CB offset was fixed at 5 meV to be consistent with sample 5. However, a valence-band offset of -6.5 meV was required to describe the data, vs 0 meV used for sample 5. It is unlikely that the two samples have significantly different values of x since both are well described using the data from the same $x=0.01$ $Zn_{1-x}Fe_xSe$ epilayer as input to the model to quantify the spin splitting in the DMS layers. A more likely scenario is that the thicker MQW sample is in a different state of strain, and hence the band offsets are somewhat different. In support of this, we note that the zero-field excitonic energy of the MQW sample is about 4 meV higher than that of the single well sample, even though well and barrier widths are comparable. This fact is hard to explain without assuming a different level of strain in the two samples.

CONCLUSIONS

We have developed a simple model which accurately predicts the behavior of excitons in shallow quantum-well systems. This model was shown to be very useful in interpreting data from single- and multiple-quantum-well systems, especially under circumstances where the valence- and/or conduction-band offsets are small compared to the exciton binding energy. The model provides quantitative predictions of excitonic energies and relative intensities, and yields a detailed description and analysis of the type-I–type-II transition and the behavior of excitons in a spin superlattice. In addition, the model also predicts and describes certain interesting phenomena, such as metastable "above-gap" excitons which should exist in certain type-II systems. Also, reentrant type-I–type-II–type-I transitions are also possible, provided the right material parameters are chosen. The formalism developed provides a framework for understanding and describing these phenomena, as well as other behavior which may be observed in the future as the study of these interesting quantum-well systems progresses.

ACKNOWLEDGMENTS

The work at SUNY was supported by NSF, Grant No. DMR8922177 and by ONR/DOD under the MFEL program. AT NRL, the work was supported by the Office of Naval Research.

*Present address: Physics Department, Chung Yuan Christian University, Chung Li, Taiwan 32023, ROC.
†Present address: MIT National Magnet Laboratory, Cambridge, MA 02139.

[1]X. Liu, A. Petrou, J. Warnock, B. T. Jonker, G. A. Prinz, and J. J. Krebs, Phys. Rev. Lett. **63**, 2280 (1989).
[2]E. Deleporte, J. M. Berroir, G. Bastard, C. Delalande, J. M. Hong, and L. L. Chang, Phys. Rev. B **42**, 5891 (1990).
[3]M. von Ortenberg, Phys. Rev. Lett. **49**, 1041 (1982).
[4]W. C. Chou, A. Petrou, J. Warnock, and B. T. Jonker, Phys.

Rev. Lett. **67**, 3820 (1991).
[5]N. Dai, H. Luo, F. C. Zhang, N. Samarth, M. Dobrowolska, and J. K. Furdyna, Phys. Rev. Lett. **67**, 3824 (1991).
[6]O. Goede, W. Heimbrodt, K. Hieke, E.-H. Gumlich, Th. Pier, B. Lunn, D. E. Ashenford, S. Jackson, and J. E. Nicholls, Superlatt. Microstruct. **12**, 363 (1992).
[7]J. F. Smyth, D. D. Awschalom, N. Samarth, H. Luo, and J. K. Furdyna, Phys. Rev. B **46**, 4340 (1992).
[8]D. D. Awschalom, J. M. Hong, L. L. Chang, and G. Grinstein, Phys. Rev. Lett. **59**, 1733 (1987).
[9]X. C. Zhang, S. K. Chang, A. V. Nurmikko, L. A. Kolodziejski, R. L. Gunshor, and S. Datta, Appl. Phys. Lett. **47**, 59 (1985).
[10]M. R. Freeman, D. D. Awschalom, J. M. Hong, and L. L. Chang, Phys. Rev. Lett. **64**, 2430 (1990).
[11]W. C. Chou, A. Petrou, J. Warnock, and B. T. Jonker, Phys. Rev. B **46**, 4316 (1992).
[12]D. D. Awschalom, M. R. Freeman, N. Samarth, H. Luo, and J. K. Furdyna, Phys. Rev. Lett. **66**, 1212 (1991).
[13]D. D. Awschalom, J. Warnock, J. M. Hong, L. L. Chang, M. B. Ketchen, and W. J. Gallagher, Phys. Rev. Lett. **62** (1989).
[14]S. K. Chang, A. V. Nurmikko, J. W. Wu, L. A. Kolodziejski, and R. L. Gunshor, Phys. Rev. B **37**, 1191 (1988).
[15]G. Bastard, E. E. Mendez, L. L. Chang, and L. Esaki, Phys. Rev. B **26**, 1974 (1982).
[16]D. S. Chemla, Helv. Phys. Acta **56**, 607 (1983).
[17]P. Harrison, J. Goodwin, and W. E. Hagston, Phys. Rev. B **46**, 12 377 (1992).
[18]A. L. Efros, Fiz. Tekh. Poluprovodn. **20**, 1281 (1986) [Sov. Phys. Semicond. **20**, 808 (1986)].
[19]E. L. Ivchenko, A. V. Kavokin, V. P. Kochereshko, G. R. Posina, I. N. Uraltsev, D. R. Yakovlev, R. N. Bicknell-Tassius, A. Waag, and G. Landwehr, Phys. Rev. B **46**, 7713 (1992).
[20]C. Delalande, Superlatt. Microstruct. **12**, 387 (1992).
[21]J. A. Gaj, J. Ginter, and R. R. Galazka, Phys. Status Solidi B **89**, 655 (1978).
[22]X. C. Liu, W. C. Chou, A. Petrou, J. Warnock, B. T. Jonker, G. A. Prinz, and J. J. Krebs, in *Proceedings of the Twentieth International Conference on the Physics of Semiconductors,* edited by E. M. Anastassakis and J. D. Joannopoulos (World Scientific, Singapore, 1990), pp. 621–624.
[23]B. T. Jonker, J. J. Krebs, S. B. Qadri, and G. A. Prinz, Appl. Phys. Lett. **50**, 848 (1987).
[24]A. Petrou, W. C. Chou, X. C. Liu, J. Warnock, and B. T. Jonker, J. Lumin. **52**, 175 (1992).